


ORIGINAL ARTICLE

Can spectral computed tomography imaging improve the differentiation between malignant and benign pulmonary lesions manifesting as solitary pure ground glass, mixed ground glass, and solid nodules?

Mai-Lin Chen, Xiao-Ting Li, Yi-Yuan Wei, Li-Ping Qi & Ying-Shi Sun 

Key Laboratory of Carcinogenesis and Translational Research (Ministry of Education/Beijing), Department of Radiology, Peking University Cancer Hospital & Institute, Beijing, China

Keywords

Computed tomography; solitary pulmonary nodule; spectral CT.

Correspondence

Ying-Shi Sun, Key Laboratory of Carcinogenesis and Translational Research (Ministry of Education/Beijing), Department of Radiology, Peking University Cancer Hospital and Institute, No. 52 Fucheng Road, Hadian District Beijing 100142, China.
Tel: +86 10 8819 6822
Fax: +86 10 8819 6822
Email: sys27@163.com

Received: 16 October 2018;

Accepted: 19 November 2018.

doi: 10.1111/1759-7714.12937

Thoracic Cancer **10** (2019) 234–242**Abstract**

Background: This study quantitatively assessed the efficacy of spectral computed tomography (CT) imaging parameters for differentiating the malignancy and benignity of solitary pulmonary nodules (SPNs) manifesting as ground glass nodules (GGNs) and solid nodules (SNs).

Methods: The study included 114 patients with SPNs (61 GGNs, and 53 SNs) who underwent CT plain and enhanced scans in the arterial (a) and venous (v) phases using the spectral imaging mode. The spectral CT imaging parameters included: iodine concentrations (IC) of lesions in the arterial (ICLa) and venous (ICLv) phases; normalized IC (NICa/NICv, normalized to the IC in the aorta); the slope of the spectral Hounsfield unit (HU) curve ($\lambda\text{HUa}/\lambda\text{HUv}$); and monochromatic CT number (CT40keVa/v , CT70keVa/v) enhancement on 40 and 70 keV images. The two-sample Mann–Whitney *U* test was used to compare quantitative parameters between malignant and benign SPNs, SNs, and GGNs.

Results: Pathology revealed 75 lung cancer cases, 3 metastatic nodules, 14 benign nodules, and 22 inflammatory nodules. Among the 53 SNs there were 37 malignant and 16 benign nodules. Among the 61 GGNs there were 41 malignant and 20 benign nodules. Overall, the CT40keVa , λHUa , CT40keVv , λHUv , and ICLv of benign SPNs were all greater than those of malignant SPNs (all $P < 0.05$). For GGNs, CT40keVa/v , CT70keVa/v , $\lambda\text{HUa}/\lambda\text{HUv}$, and ICLv of malignant GGNs were all lower than those of benign GGNs.

Conclusion: Spectral CT imaging is a more promising method for distinguishing malignant from benign nodules, especially in nodules manifesting as GGNs in contrast-enhanced scanning.

Introduction

The incidence of solitary pulmonary nodules (SPNs) has constantly increased and incorrect diagnosis remains a hot topic in clinical practice. Conventional chest contrast-enhanced computed tomography (CT) remains the standard method for identifying suspected lung cancer from detected pulmonary nodules. Contrast-enhanced CT images are used to characterize pulmonary nodules based on different morphological signs and enhancement patterns. Deep lobulated or coarse spiculated margins and

maximum attenuation of 20–60 Hounsfield units (HU)¹ often indicate malignancy or central dense calcifications, while maximum attenuation of ≤ 15 HU¹ often serves as a clue of benignity. However, oversimplified morphologic appearance or enhanced values are unreliable for deriving an accurate diagnosis of lung cancer from different kinds of lung nodules in clinical practice.

There is considerable overlap between benign and malignant SPNs in terms of enhancement patterns in conventional CT images.¹ Spectral CT is used by calculating the energy

dependence of the X-ray attenuation coefficient by analyzing and amplifying the mechanism and detail of traditional CT imaging, with multiple parameters acquired by means of monochromatic spectral images at energy levels ranging from 40 to 140 keV, as well as accurate material decomposition images, such as monochromatic imaging, material decomposition images, and spectral HU curve.^{2,3} Moreover, the monochromatic spectral images of single energy levels provide information about the attenuation changes in different materials as a function of X-ray photon energy.^{2,4} Spectral CT material decomposition images enable the iodine component of SPNs to be measured on iodine-enhanced images, which is considered comparable to the real value (net enhancement) of the extent of enhancement.^{2,3,5}

To identify lung nodules using spectral CT images, several studies have used multiple parameters, including iodine concentrations (IC), normalized iodine concentrations (NIC), CT numbers of 40 or 70 keV monochromatic images (CT40keV or CT70keV), and the slope of the spectral attenuation curve (λ HU) to distinguish among inflammatory, granuloma, benign nodules, and malignant tumors.^{5–11} These studies showed that spectral CT is one of the most promising imaging techniques with potential clinical applications, although controversy and disagreement remain. Thus, our aim was to prospectively evaluate the usefulness of these parameters (IC, NIC, CT40keV, CT70keV, and λ HU) for differentiating malignant and benign SPNs manifesting as pure ground glass nodules (pGGNs), mixed ground glass nodules (mGGNs), and solid nodules (SNs).

Methods

Patients

From January to August 2018, a total of 114 patients (54 men, 60 women, age range: 42–81 years, mean age 60.2 years \pm 8.1), were prospectively enrolled in the study. The Medical Ethical Committee of Peking University Cancer Hospital and Institute approved the research protocol and written informed consent was obtained from all patients. Patients were selected according to the following inclusion criteria: presence of a solitary intrapulmonary nodule (pGGN, mGGN, or SN), an existing lesion \geq 6 mm, and no contraindications to the administration of iodinated contrast material. The exclusion criteria were: patients with nodules of a maximum diameter < 6 mm, patients aged under 18 years, pregnant patients, or patients who declined to participate.

Computed tomography (CT) examinations

Computed tomography examinations were performed using two-phase enhanced CT scanning using the spectral imaging mode on a Revolution Xstream CT scanner

(GE Healthcare, Madison, WI, USA). Patients were injected with 40/50 mL (\leq 70 kg body weight, 40 mL; > 70 kg body weight, 50 mL) Iopromide (Ultravist 300; Bayer Schering Pharma AG, Guangzhou, China) at a flow rate of 5/6 mL/s (\leq 70 kg body weight, 5 mL/s; > 70 kg body weight, 6 mL/s), followed by 30 mL saline solution at the same injection rate. A GSI exam of the entire chest was performed with scan delays of 30 and 90 seconds after the start of contrast injection during the arterial (a) and portal venous (v) phases, respectively. No serious injection complications or issues occurred.

The acquisition parameters were: helical tube rotation time 0.6 seconds, helical pitch 0.985, tube current of 600 mA, 512×512 pixel matrix, SFOV 500 mm and collimation 40 mm, slice thickness of 5 mm, and slice gap of 5 mm. Contiguous axial images of 2.5 and 1.25 mm thickness were generated with a soft tissue kernel (standard) monochromatic with the GSI data file at default energy levels of 40 and 70 KeV. The CT dose index volume (CTDIvol) for GSI acquisition was 4.73 mGy.

Quantitative analysis of spectral CT images

All data were processed and analyzed using the GSI Volume Viewer software package at AW4.7 workstation (GE Healthcare). A radiologist with 10 years of experience in chest CT diagnosis took the quantitative measurements to analyze the monochromatic and material decomposition images. During data analysis, the radiologist amplified the display field of view by 15 or 20 cm to better select the region of interest (ROI). The ROI was selected at the maximum section of the lesion and carefully placed in an area that avoided calcification, liquefaction, or necrosis, away from pulmonary vessels and bronchi, and as large a region as possible to reduce noise (0.50 pixels). All measurements were repeated three times at the three contiguous imaging levels and average values were calculated to ensure consistency.

Three types of images were reconstructed from the spectral CT acquisition for analysis: spectral curve image, iodine-based material decomposition images, and monochromatic image obtained at energies ranging from 40 to 140 keV (Fig 1). Net CT numbers at energy levels of 40 and 70 keV were chosen at both a and v phases (CT40keVa, CT70keVa and CT40keVv, CT70keVv) to measure. In the iodine density image derived from the iodine/water based material decomposition image, the IC of lesions (ICLa/ ICLv) in double-phase enhanced scans were measured. In the same slice, the IC in the aorta descendens or subclavian artery (ICA) was also measured. The normalized IC (NICa and NICv), which is the IC ratio in the lesion and aorta descendens (NIC = ICL/ICA), was calculated. These IC parameters, ICLa, ICLv, ICAa, ICAv, NICa and NICv, are calculated in the a and v phases,

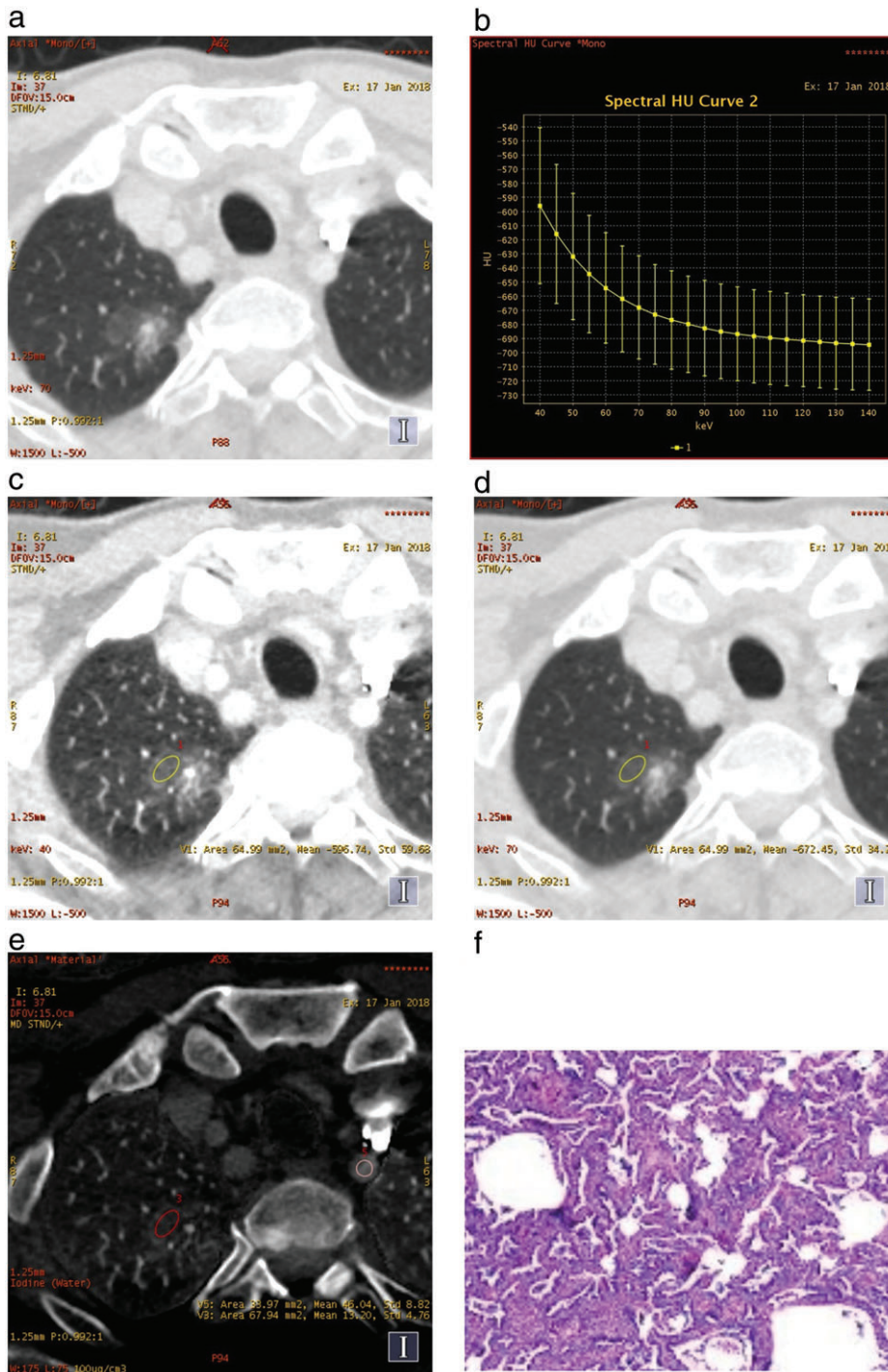


Figure 1 A mixed ground glass nodule in (a) the right upper lobe, (b) the spectral curve, (c) the monoenergetic computed tomography (CT) number obtained at 40 keV and (d) 70 keV energy levels on transverse monoenergetic CT image, and (e) iodine concentrations of the lesion and the left subclavian artery on iodine-based material decomposition images, obtained from single spectral CT acquisition (section thickness 1.25 mm) in the arterial phase. (f) Lepidic predominant adenocarcinoma in a 54-year-old man was confirmed by postoperative pathology.

respectively. The slope of the spectral HU curve (λ HU) was assessed at the 40–70 keV region using the equation λ HU = (40–70 keV) HU/70–40, based on previous studies. λ HU_a = (40–70 keV_a) HU/70–40 and λ HU_v = (40–70 keV_v) HU/70–40 were calculated. In total 12 variables were analyzed, as shown in Tables 1 and 2.

Statistical analysis

Data were transformed using a Box-Cox power transformation by Statistica 12 (Dell Inc., Round Rock, TX, USA) to minimize the influence of extreme values or non-normal distribution. Parameters were expressed as

Table 1 Raw variables for differentiating general benign from malignant SPNs

Parameters	Benign (n = 36)	Malignant (n = 78)	P
CT40keVa	102.23 ± 156.24	-16.56 ± 248.21	0.021
CT70keVa	2.65 ± 135.46	-69.03 ± 355.22	0.162
ICLa	16.96 ± 8.77	14.33 ± 6.41	0.057
ICAA	53.89 ± 30.77	46.89 ± 29.33	0.228
NICa	0.45 ± 0.36	0.40 ± 0.25	0.923
λHUa	99.57 ± 48.50	78.97 ± 34.56	0.015
CT40keVv	102.07 ± 152.64	-15.09 ± 239.58	0.009
CT70keVv	-0.96 ± 133.79	-96.27 ± 229.42	0.163
ICLv	18.22 ± 8.65	13.58 ± 4.37	0.002
ICAv	25.11 ± 5.38	25.84 ± 5.74	0.472
NICv	0.72 ± 0.36	0.64 ± 0.40	0.120
λHUv	103.03 ± 48.84	81.18 ± 32.20	0.006

CT40keVa and CT70keVa, monochromatic computed tomography number enhancement on 40 and 70 keV images in the arterial (a) phase, respectively; CT40keVv and CT70keVv, monochromatic computed tomography number enhancement on 40 and 70 keV images in the venous (v) phase, respectively; HU, Hounsfield unit; IC, iodine concentration; NIC, normalized IC; SPNs, solitary pulmonary nodules.

mean ± standard deviation and were tested for normal distribution using the Kolmogorov–Smirnov test. If parameters did not obey normal distribution, the Mann–Whitney *U* test was performed to compare the parameters between the benign and malignant groups, with a Bonferroni adjustment for multiple comparisons. A *P* value of < 0.05 indicated statistical significance. SPSS version 18 was used to perform statistical analysis (SPSS Inc., Chicago, IL, USA).

Table 2 Raw variables for differentiating general benign from malignant SNs

Parameters	Benign (n = 16)	Malignant (n = 37)	P
CT40keVa	139.61 ± 49.14	138.70 ± 43.36	0.713
CT70keVa	49.65 ± 18.82	116.40 ± 362.79	0.121
ICLa	15.84 ± 5.83	14.68 ± 6.15	0.450
ICAA	59.87 ± 31.61	48.02 ± 29.87	0.181
NICa	0.35 ± 0.25	0.38 ± 0.20	0.237
λHUa	89.96 ± 31.94	78.16 ± 33.84	0.222
CT40keVv	143.40 ± 41.67	135.88 ± 36.73	0.535
CT70keVv	51.70 ± 16.93	53.83 ± 10.28	0.771
ICLv	15.77 ± 4.99	13.93 ± 4.36	0.245
ICAv	25.72 ± 5.77	24.81 ± 5.42	0.656
NICv	0.62 ± 0.18	0.62 ± 0.18	0.846
λHUv	91.70 ± 29.56	82.05 ± 29.77	0.222

CT40keVa and CT70keVa, monochromatic computed tomography number enhancement on 40 and 70 keV images in the arterial (a) phase, respectively; CT40keVv and CT70keVv, monochromatic computed tomography number enhancement on 40 and 70 keV images in the venous (v) phase, respectively; HU, Hounsfield unit; IC, iodine concentration; NIC, normalized IC; SNs, solitary nodules.

Results

We analyzed 114 nodules (78 malignant; 36 benign) from 114 patients. The lesion characteristics are shown in Table 3. Lesion size varied considerably: the mean diameter was 21 mm (range: 6–51 mm). Benign or malignant status was verified by tissue sampling, surgery (50.9%), biopsy (39.5%), and diagnostic treatment follow-up (9.6%). There were 53 SNs and 61 GGNs. The malignant nodules consisted of: lung adenocarcinoma (54.4%), squamous cell carcinoma (3.5%), small cell carcinoma (4.4%), and metastases (2.6%). The benign nodules consisted of: inflammatory (19.3%) and granuloma (11.4%). The inflammatory nodules consisted of: 16 pneumonitis, 3 lung abscess, and 3 focal-organizing pneumonia (Table 3).

Table 3 Review of baseline population and lesion characteristics in the general, SN, and GGN cohorts

Variable	Total (n = 114)	SNs (n = 53)	GGNs (n = 61)
Age (years)	60.2 ± 8.1	58.70 ± 10.36	53.6 ± 7.6
Gender			
Male	54 (47.4%)	25 (47.2%)	29 (47.5%)
Female	60 (52.6%)	28 (52.8%)	32 (52.5%)
Diameter (mm)	2.1 ± 1.25	2.6 ± 1.5	1.9 ± 1.1
Diagnostic technique			
Biopsy	45 (39.5%)	25 (47.2%)	20 (32.8%)
Surgery	58 (50.9%)	23 (43.4%)	35 (57.4%)
Follow-up	11 (9.6%)	5 (9.4%)	6 (9.8%)
Location			
Central	21 (18.4%)	18 (34.0%)	3 (4.9%)
Peripheral	93 (81.6%)	35 (66.0%)	58 (95.1%)
Final diagnosis			
Benign	36 (31.6%)	25 (47.2%)	11 (18.0%)
Malignant	78 (68.4%)	28 (52.8%)	50 (82.0%)
Malignant lesions			
Adenocarcinoma	62 (54.4%)	16 (30.2%)	46 (75.4%)
Squamous cell carcinoma	4 (3.5%)	4 (7.5%)	0
Small cell carcinoma	5 (4.4%)	5 (9.4%)	0
Mucous adenocarcinoma	1 (0.9%)	1 (1.9%)	0
Large cell carcinoma	1 (0.9%)	1 (1.9%)	0
Sarcomatoid carcinoma	1 (0.9%)	1 (1.9%)	0
Carcinoid			0
Metastatic carcinoma	1 (0.9%)	1 (1.9%)	0
Benign lesions			
Inflammatory	22 (19.3%)	11 (20.8%)	11 (18.0%)
Granuloma	13 (11.4%)	9 (17.0%)	4 (6.6%)
Sclerosing pulmonary cell tumor	1 (0.9%)	1 (1.9%)	0

GGN, ground glass nodule; SN, solid nodule.

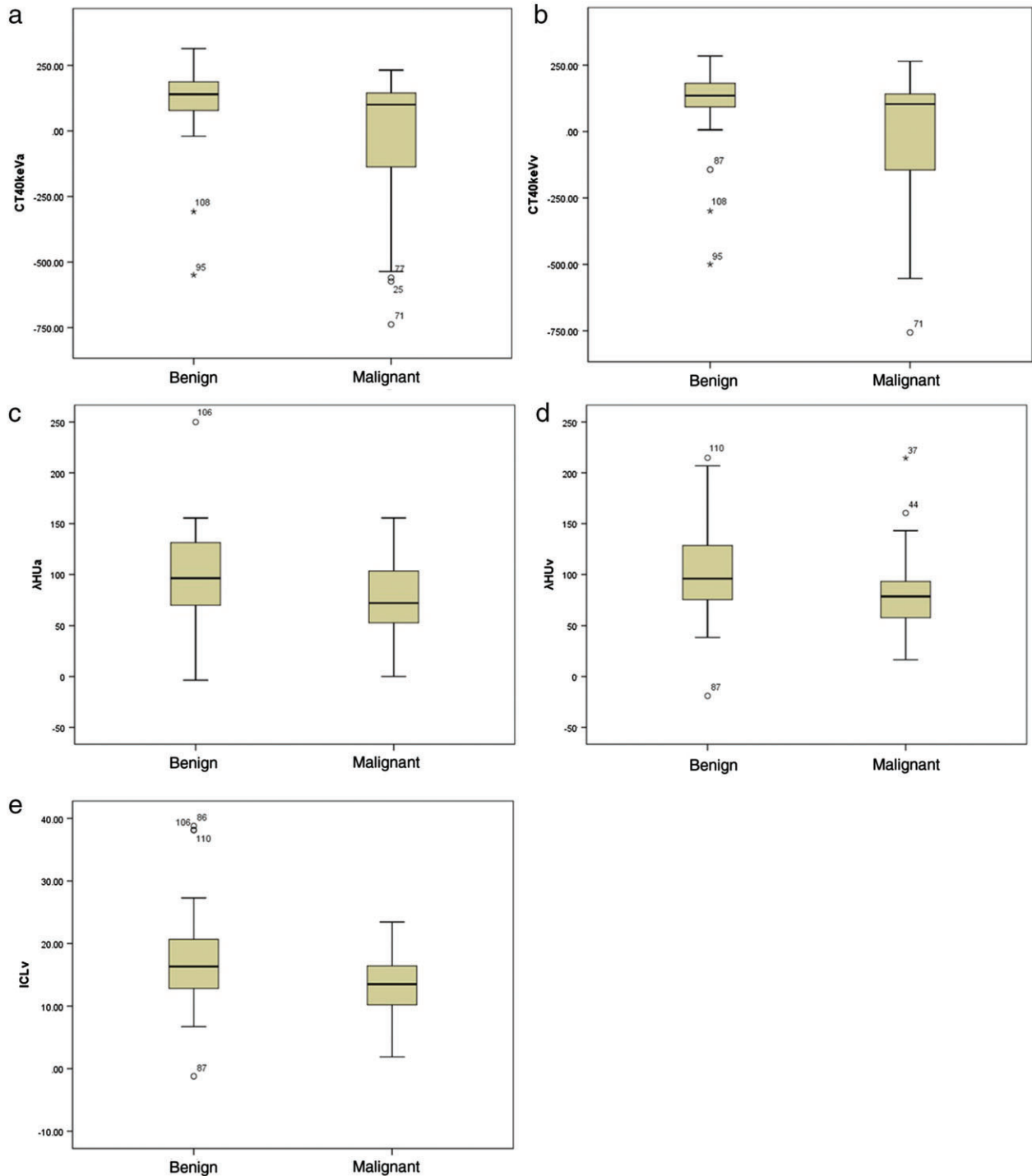


Figure 2 The graphs show box-whisker plots for comparisons between benign and malignant solitary pulmonary nodules (SPNs): (a) monochromatic computed tomography (CT) number enhancement on 40 and keV images in CT40keVa and (b) CT40keVv, and Hounsfield unit (HU) curves (c) λHUa and (d) λHUv in the arterial (a) and venous (v) phases, respectively; and (e) the iodine concentration in the v phase (ICLv). Box-whisker plots are shown, in which the lower box boundary indicates the 25th percentile, the line within the box marks the median, and the top box boundary indicates the 75th percentile. Error bars below and above the boxes indicate the 10th and 90th percentiles, respectively. Other data are represented as individual dots. The CT40keVa, CT40keVv, λHUa, λHUv and ICLv of malignant SPNs were significantly lower than those of benign SPNs (all $P < 0.05$).

Table 4 Raw variables for differentiating general benign from malignant GGNs

Parameters	Benign (n = 20)	Malignant (n = 41)	P
CT40keVa	67.04 ± 210.23	-142.14 ± 259.84	0.004
CT70keVa	-41.58 ± 179.11	-223.28 ± 241.60	0.004
ICLa	18.02 ± 10.92	14.29 ± 6.54	0.097
ICAA	48.26 ± 28.96	46.24 ± 30.62	0.834
NICa	0.53 ± 0.42	0.42 ± 0.29	0.530
λHUa	108.62 ± 59.75	81.14 ± 34.82	0.038
CT40keVv	63.17 ± 204.09	-136.21 ± 247.64	0.004
CT70keVv	-50.52 ± 173.63	-216.19 ± 235.50	0.012
ICLv	20.53 ± 10.71	13.55 ± 4.08	0.002
ICAv	24.53 ± 5.09	26.96 ± 5.87	0.123
NICv	0.81 ± 0.45	0.68 ± 0.52	0.075
λHUv	113.69 ± 60.85	81.98 ± 33.46	0.009

CT40keVa and CT70keVa, monochromatic computed tomography number enhancement on 40 and 70 keV images in the arterial (a) phase, respectively; CT40keVv and CT70keVv, monochromatic computed tomography number enhancement on 40 and 70 keV images in the venous (v) phase, respectively; GGNs, ground-glass nodules; HU, Hounsfield unit; IC, iodine concentration; NIC, normalized IC.

Comparison of IC, NIC, and λHU between benign and malignant SPNs in the general cohort was conducted. In malignant SPNs, the CT40keVa, CT40keVv, λHUa, λHUv, and ICLv were significantly lower than in benign SPNs (all $P < 0.05$) (Table 1, Fig 2). The CT40keVa, λHUa, CT40keVv, λHUv, and ICLv in benign and malignant nodules were: 102.23HU ± 156.24 versus -16.56HU ± 248.2, 99.57 ± 48.50 versus 78.97 ± 34.56, 102.07HU ± 152.64 versus -15.09HU ± 239.58, 18.22mg/mL ± 8.65 versus 13.58mg/mL ± 4.37, and 103.03 ± 48.84 versus 81.18 ± 32.20, respectively.

In the SN subgroup, 53 nodules (28 malignant, 25 benign) were assessed. Malignant SNs included: adenocarcinoma (30.2%), squamous cell carcinoma (7.5%), small cell carcinoma (9.4%), and metastases (5.7%). There were no statistically significant differences in the IC, NIC, and λHU of malignant SPNs in both a and v phases compared to those of benign SPNs. (Table 2).

In the GGN (pGGN and mGGN) subgroup, 61 nodules (28 malignant, 25 benign) were assessed (Table 3). The malignant nodules included were mainly adenocarcinomas (75.4%). The raw variables for differentiating benign from malignant GGNs are shown in Table 4. There were statistically significant differences between the IC, NIC, and λHU of malignant SPNs compared to benign SPNs. The CT40keVa, CT40keVv, CT70keVa, CT70keVv, λHUa, λHUv, and ICLv of malignant nodules were all lower than those of benign nodules (Fig 3). The CT40keVa, CT40keVv, CT70keVa, CT70keVv, λHUa, λHUv, and ICLv in benign and malignant nodules were: 67.04HU ± 210.23 versus -142.14HU ± 259.84; 63.17HU ± 204.09 versus -136.21HU ± 247.64; -41.58HU ± 179.11 versus -223.28HU ± 241.60; -50.52HU ± 173.63 versus

-216.19 ± 235.50; 108.62 ± 59.75 versus 81.14 ± 34.82; 113.69 ± 60.85 versus 81.98 ± 33.46, and 20.53 mg/mL ± 10.71 versus 13.55 mg/mL ± 4.08, respectively.

Discussion

It is well known that conventional CT imaging plays an important role in the diagnostic differentiation of lung nodules. Spectral CT imaging has the potential to provide multiple parameters, such as monochromatic and material decomposition imaging, to differentiate between benign and malignant SPNs. Some studies have reported that the iodine-related parameters (IC) of malignant SPNs are significantly higher than those of benign SPNs,^{8,9} while others have reported that the IC and λHU in a pneumonia group were higher than in a malignant tumor group.⁵ However, our research results indicated that spectral CT images with iodine quantification have a different value for distinguishing SNs and GGNs, and may be more useful for differentiating benign and malignant GGNs than SNs.

In previous studies, net CT value increases in contrast-enhanced scans have been used to differentiate benign and malignant characteristics of SPNs, with a cutoff value of 15 or 20 HU.¹ Lung tumors often show rapid and strong contrast enhancement because of the high vascularity in tumors and the interstitial accumulation of contrast material by means of the increased permeability of tumor capillaries.¹² CT numbers on the iodine-enhanced image and the degree of enhancement show good agreement (intra-class correlation coefficients: 0.83 and 0.91, respectively) with CT numbers on virtual non-enhanced and non-enhanced weighted average images.³ In a spectral CT imaging study, the net CT number increases of malignant SPNs in the monochromatic energy level images after contrast enhancement were higher than those of benign SPNs.^{6,8,9,13} Some studies concluded that net CT number of 70keV monochromatic images in a (CT70keVa) and v (CT70keVv) phases indicated suitable enhancement in tumors,⁸ while others suggested that the net CT number of 40 keV (CT40keV) was a good choice, although the scan times were different in the a and v phases after injection of the contrast medium. Therefore, our study included two parameters in the double phase, CT40keV and CT70keV, to differentiate benign and malignant SPNs. In all nodules, CT40keVa and CT40keVv were higher in benign than malignant nodules (Fig 2a,b), which is a more apt differentiation of the nature of the nodules. Similarly for GGNs, CT40keV was used to perform differential diagnosis of benign and malignant nodules (Fig 3a,b). The variation in CT70keV between benign and malignant GGNs was statistically significant, while CT70keVa and

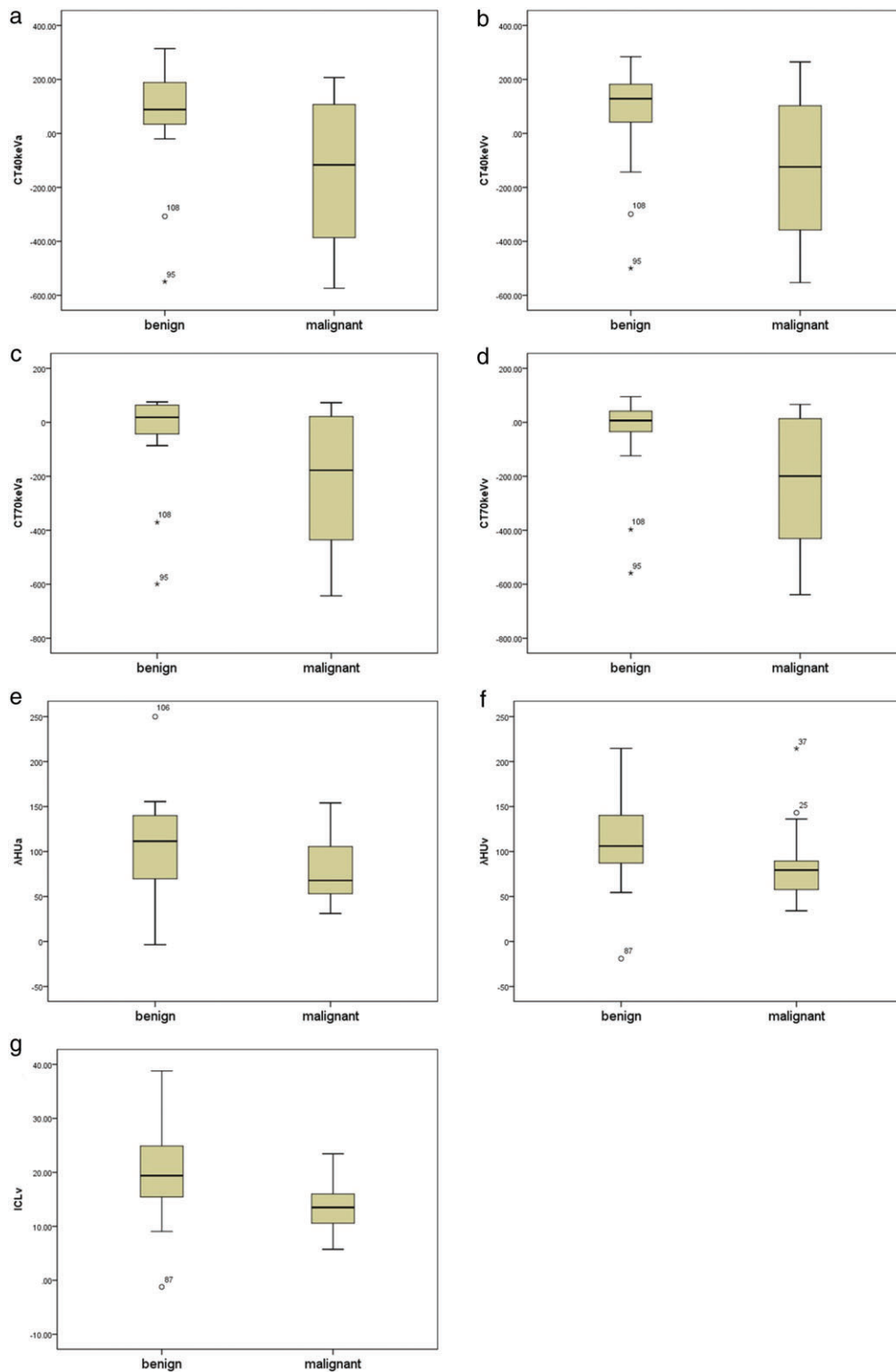


Figure 3 The graphs show box-whisker plots for comparisons between benign and malignant pure and mixed ground glass nodules (GGNs): monochromatic CT number enhancement on 40 and 70 keV images in (a) CT40keVa, (b) CT40keVv, (c) CT70keVa, (d) CT70keVv, and Hounsfield unit (HU) curves (e) λHUa and (f) λHUv, in the arterial (a) and venous (v) phases, respectively; and (g) the iodine concentration in the v phase (ICLv). Box-whisker plots are shown, in which the lower box boundary indicates the 25th percentile, the line within the box marks the median, and the top box boundary indicates the 75th percentile. Error bars below and above the boxes indicate the 10th and 90th percentiles, respectively. Other data are represented as individual dots. The CT40keVa, CT40keVv, CT70keVa, CT70keVv, λHUa, λHUv, and ICLv of malignant GGNs were all lower than those of benign GGNs (all $P < 0.05$).

CT70keVv were higher in benign compared to the malignant nodules (Fig 3c,d).

Thus, we used the 40–70 keV region to define λ HU and assess the slope of the energy attenuation curve of an X-ray beam passing through the nodules,^{14,15} while previous studies used 40–100 keV, 70–100 keV or 100–140 keV regions.^{5,9,13} The use of λ HU, including λ HUa and λ HUv, in this investigation was specific to spectral CT imaging and thus was a feasible method to distinguish between general malignant and benign nodules (Fig. 2c,d). Using the λ HUa and λ HUv to distinguish benign from malignant GGNs in the lungs, benign GGNs showed statistically significantly higher λ HUs (Fig 3e,f).

The nodule IC directly reflects the blood supply situation in the lesion. Several studies have compared the CT number of pulmonary nodules on iodine-enhanced images with those on enhanced weighted average images. The CT number on iodine-enhanced images revealed that malignant nodules have significantly higher enhancement than benign nodules ($P < 0.05$), with higher diagnostic sensitivity and accuracy.^{8,9,16–18} Our results revealed that for these general nodules, the ICLv was higher in the benign than in the malignant group (Fig 2e). For GGNs, the ICLv decreased in malignant nodules at the same rate it increased in benign nodules (Fig 3g).

Our results were inconsistent with previous research in that the two parameters, λ HU and IC, in benign nodules were lower than in malignant nodules.^{5,9,13} There are several reasons to explain this paradoxical condition. A major reason may be the different sample populations used, as previous studies focused on SNs, while our study analyzed SNs (46.5%) and GGNs (53.5%). GGNs and SNs were also investigated using spectral CT imaging to determine benignity or malignancy. Kawai *et al.* addressed the feasibility of using spectral CT imaging to differentiate GGNs, by performing a phantom study with artificial GGNs to analyze differences in calcium and iodine concentrations, and then applying the spectral CT technique to clinical cases with lung lesions.¹⁹ Our results emphasize that spectral CT parameters CT40keV, CT70keV, and λ HU in the double phase and IC in the v phase were advantageous for separating malignant and benign GGNs, as these parameters were significantly elevated in benign compared to malignant GGNs. Another related condition, benign nodules were principally inflammatory (61.1%). The IC was highest in the active inflammatory group, followed by the malignant group, which has been confirmed by previous studies.^{5,18,20} The active inflammatory nodule is stimulated by inflammatory agents, which leads to the arteriole and blood capillary becoming more obviously dilated and the vascular permeability increased. Inflammatory edema tissues compress the drainage vein and increase the hydrostatic

pressure of the tissues, and block the blood reflux more obviously in benign than in malignant nodules. Therefore, the active inflammatory nodule shows earlier and more obvious reinforcement.^{21,22} The IC is not only closely related to the blood supply, but also influenced by various factors, including the total dose of contrast medium, flow rate of injection, delayed scan time, and individual differences in circulation. In this investigation, the total dose of contrast medium (40/50 mL) was lower and the flow rate of injection (5/6 mL/s) was faster than in previous studies, which may be a third factor to explain the differences in our results. These factors may explain why our spectral CT variables did not meet statistical significance for differentiating benign and malignant SNs. Further studies should be conducted to confirm our results.

This study has several limitations. Firstly, this was a single center study.²³ Secondly, the relatively small study population limited our subgroup results; thus further studies using larger sample sizes need to be performed. Thirdly, the parameters were calculated from the GGN with a skip attenuation range between -800 and -50 HU; however, the reliability of this method for GGNs with higher attenuation has not yet been clarified and should be investigated further. Finally, we used different total doses of contrast medium and flow rates of injection than previous studies; therefore, non-normalization should be applied to raw measurements.

In conclusion, spectral CT imaging is useful to acquire multiple quantitative parameters for distinguishing malignant solitary pulmonary nodules from benign. These parameters are highly practicable for the clinical diagnosis of benign and malignant GGNs.

Acknowledgments

This work was supported by Beijing Municipal Administration of Hospitals Clinical Medicine Development of Special Funding Support (No. ZYLX201803), the Beijing Million Talents Project (No. 2017A13) and the Beijing Natural Science Foundation of China (Grant no. 7172049).

Disclosure

No authors report any conflict of interest.

References

- Ohno Y, Nishio M, Koyama H *et al.* Dynamic contrast-enhanced CT and MRI for pulmonary nodule assessment. *AJR Am J Roentgenol* 2014; **202** (3): 515–29.
- Johnson TR, Krauss B, Sedlmair M *et al.* Material differentiation by dual energy CT: Initial experience. *Eur Radiol* 2007; **17** (6): 1510–7.

- 3 Chae EJ, Song J-W, Seo JB, Krauss B, Jang YM, Song K-S. Clinical utility of dual-energy CT in the evaluation of solitary pulmonary nodules: Initial experience. *Radiology* 2008; **249** (2): 671–81.
- 4 De Cecco CN, Darnell A, Rengo M *et al.* Dual-energy CT: Oncologic applications. *Am J Roentgenol* 2012; **199** (5 Suppl): S98–S105.
- 5 Wang G, Zhang C, Li M, Deng K, Li W. Preliminary application of high-definition computed tomographic gemstone spectral imaging in lung cancer. *J Comput Assist Tomogr* 2014; **38** (1): 77–81.
- 6 Hou WS, Wu HW, Yin Y, Cheng JJ, Zhang Q, Xu JR. Differentiation of lung cancers from inflammatory masses with dual-energy spectral CT imaging. *Acad Radiol* 2015; **22**: 337–44.
- 7 Kim H, Park CM, Lee SM, Lee H-J, Goo JM. A comparison of two commercial volumetry software programs in the analysis of pulmonary ground-glass nodules: Segmentation capability and measurement accuracy. *Korean J Radiol* 2013; **14**: 683–91.
- 8 Zhang Y, Cheng J, Hua X *et al.* Can spectral CT imaging improve the differentiation between malignant and benign solitary pulmonary nodules? *PLoS One* 2016; **11**: e0147537.
- 9 Xiao H, Liu Y, Tan H *et al.* A pilot study using low-dose spectral CT and ASIR (adaptive statistical iterative reconstruction) algorithm to diagnose solitary pulmonary nodules. *BMC Med Imaging* 2015; **15**: 54.
- 10 Yang F, Dong J, Wang X, Fu X, Zhang T. Non-small cell lung cancer spectral computed tomography quantitative parameters for preoperative diagnosis of metastatic lymph nodes. *Eur J Radiol* 2017; **89**: 129–35.
- 11 Li X, Meng X, Ye Z. Iodine quantification to characterize primary lesions, metastatic and non-metastatic lymph nodes in lung cancers by dual energy computed tomography: An initial experience. *Eur J Radiol* 2016; **85**: 1219–23.
- 12 Li GJ, Gao J, Wang GL, Zhang CQ, Shi H, Deng K. Correlation between vascular endothelial growth factor and quantitative dual-energy spectral CT in non-small-cell lung cancer. *Clin Radiol* 2016; **71**: 363–8.
- 13 Schaefer JF, Vollmar J, Schick F *et al.* Solitary pulmonary nodules: Dynamic contrast-enhanced MR imaging—Perfusion differences in malignant and benign lesions. *Radiology* 2004; **232** (2): 544–53.
- 14 Karcaaltincaba M, Aykut A. Dual-energy CT revisited with multidetector CT: Review of Principles and clinical applications. *Diagn Interv Radiol* 2011; **17** (3): 181–94.
- 15 Remy-Jardin M, Faivre JB, Pontana F *et al.* Thoracic applications of dual energy. *Radiol Clin North Am* 2010; **48** (1): 193–205.
- 16 Lee SH, Hur J, Kim YJ, Lee HJ, Hong YJ, Choi BW. Additional value of dual-energy CT to differentiate between benign and malignant mediastinal tumors: An initial experience. *Eur J Radiol* 2013; **82** (11): 2043–9.
- 17 Swensen SJ, Viggiano RW, Midthun DE *et al.* Lung nodule enhancement at CT: Multicenter study. *Radiology* 2000; **214** (1): 73–80.
- 18 Henzler T, Shi J, Jafarov H *et al.* Functional CT imaging techniques for the assessment of angiogenesis in lung cancer. *Transl Lung Cancer Res* 2012; **1** (1): 78–83.
- 19 Kawai T, Shibamoto Y, Hara M, Arakawa T, Nagai K, Ohashi K. Can dual-energy CT evaluate contrast enhancement of ground-glass attenuation? Phantom and preliminary clinical studies. *Acad Radiol* 2011; **18**: 682–9.
- 20 Lin J, Zhang L, Zhang C, Yang L, Lou HN, Wang ZG. Application of gemstone spectral computed tomography imaging in the characterization of solitary pulmonary nodules: Preliminary result. *J Comput Assist Tomogr* 2016; **40**: 907–11.
- 21 Yamashita K, Matsunobe S, Tsuda T *et al.* Solitary pulmonary nodule: Preliminary study of evaluation with incremental dynamic CT. *Radiology* 1995; **194**: 399–405.
- 22 Zhang M, Kono M. Solitary pulmonary nodules: Evaluation of blood flow patterns with dynamic CT. *Radiology* 1997; **205**: 471–8.
- 23 Harders SW, Madsen HH, Nellemann HM *et al.* dynamic contrast-enhanced CT in suspected lung cancer: Quantitative results. *Br J Radiol* 2013; **86** (2013): 0257.